Supporting Information for "Intercomparison of atmospheric carbonyl sulfide (TransCom-COS; Part Two): Evaluation of optimized fluxes using ground-based and aircraft observations"

Jin Ma[1], Marine Remaud[2], Philippe Peylin[2], Prabir Patra[4], Yosuke Niwa[5,6], Christian Rodenbeck[7], Mike Cartwright[8,9], Jeremy J. Harrison[8,9], Martyn Chipperfield[10,11], Richard J. Pope[10,11], Christopher Wilson[10,11], Sauveur Belviso[2], Stephen A. Montzka[12], Isaac Vimont[12], Fred Moore[12], Elliot L. Atlas[13], Efrat Schwartz[14], Maarten C. Krol[1,3]

[1]Institute for Marine and Atmospheric Research, Utrecht University, Utrecht, The Netherlands

[2]Laboratoire des Sciences du Climat et de l'Environnement, CEA-CNRS-UVSQ, IPSL, Gif-sur-Yvette, France

[3]Meteorology and Air Quality, Wageningen University & Research, Wageningen, The Netherlands

[4]Research Institute for Global Change, JAMSTEC, Yokohama 236-0001, Japan

[5]National Institute for Environmental Studies, Tsukuba, Japan

[6]Meteorological Research Institute, Japan Meteorological Agency, Tsukuba, Japan

[7]Max Planck Institute for Biogeochemistry, Jena, Germany

[8]School of Physics and Astronomy, Space Park Leicester, University of Leicester, Leicester, UK

[9]National Centre for Earth Observation, Space Park Leicester, University of Leicester, Leicester, UK

[10]School of Earth and Environment, University of Leeds, Leeds, UK

[11]National Centre for Earth Observation, University of Leeds, Leeds, UK

[12]Global Monitoring Laboratory, National Oceanic & Atmospheric Administration, Boulder, USA

[13]Rosenstiel School of Marine and Atmospheric Science, University of Miami, Miami, Florida, USA

[14]Earth and Planetary Sciences, Weizmann Institute of Science, Rehovot, Israel

July 22, 2023, 7:26pm

Contents of this file

1. Text S1 to S5

2. Figures S1 to S19 (Note that Figs. S1, S2, and S8 are not in Text S1 to S5.)

S1. Model adjustments w.r.t. NOAA surface network

All model simulations start from zero COS mole fractions. Applying the optimized fluxes leads to a slightly increasing trend in simulated mole fractions. We introduce a simple adjustment, such that the simulated COS abundances can be compared to NOAA surface observations. The output of the uncorrected model simulations is shown in Fig. S4. The average budget imbalance of 21.3 GgS a^{-1} for OPT-TM5 and 4.5 GgS a^{-1} for OPT-LMDz lead to positive trends of 4.6 and 1.0 pmol mol^{-1} a^{-1}, respectively. We removed these trends from the simulations and added 485 pmol mol^{-1}, and the results are shown in Fig. S5. The resulting model time series are compared to the GIF measurements in Fig. S6.

The meridional gradients w.r.t. NOAA surface observations for each adjusted model simulation are shown in Fig. S7.

S2. The monthly mean of optimized fluxes

The optimized fluxes are averaged monthly and meridionally to show the spatial and temporal variations and the difference between OPT-TM5 and OPT-LMDz fluxes. The difference between the two optimized fluxes is presented in Fig. S3. The OPT-TM5 flux has a stronger seasonal cycle than the OPT-LMDz flux.

S3. Model simulations of NOAA aircraft stations

The NOAA aircraft platform covers 13 stations over North America, including Alaska. Fig. S9 shows the vertical gradient, of COS for each NOAA aircraft station over North America, averaged over three monthly periods, along with the results from all model simulations.

S4. Model simulations of the HIPPO and ATom measurements

All individual model simulations of the meridional and vertical COS distribution are compared to HIPPO and ATom measurements. The HIPPO campaigns mainly covered the Pacific Ocean and some of the North American continent. Hence, we show the distributions over the Pacific Ocean in Fig. S10 and the vertical profiles in Fig. S11.

The ATom campaigns covered the Pacific and Atlantic Oceans and parts of North American continent, and we show the distributions over the Pacific and Atlantic Oceans. Fig. S13 shows the simulated meridional distributions compared to ATom over the Pacific Ocean. Fig. S12 shows the simulated meridional distributions compared to ATom over the Atlantic Ocean. Fig. S14 shows the simulated vertical profiles compared to ATom over the Atlantic Ocean and Fig. S15 shows the modeled vertical profiles compared to ATom over the Pacific Ocean.

The diagnostic information about ATom campaign 4 is shown in Fig. S16. The ATom4 profiles are binned to six latitude bins. In the tropics, the observations are close to the modelled profiles in the free troposphere (above 2 km). Upper atmospheric observations decrease at higher latitudes, while model profiles are flat. Likely, the sampled air masses are mixed with stratospheric air, which brings down air with lower COS mole fractions.

S5. Control scenario performance compared with HIPPO and ATom

The control scenario is described in Remaud et al. (2023) as the first part of TransCom-COS inter-comparison project.

At HIPPO and ATom campaigns, the control scenarios are depicted in Fig. S17, S18, and S19 as meridional gradient. They show that the control scenario underestimates the COS abundance in the SH from the HIPPO and ATom flights, and slightly overestimates measurements at high latitudes in the NH.

References

Remaud, M., Ma, J., Krol, M., Abadie, C., Cartwright, M. P., Patra, P., ... others (2023). Intercomparison of atmospheric carbonyl sulfide (transcom-cos; part one): Evaluating the impact of transport and emissions on tropospheric variability using ground-based and aircraft data. *Journal of Geophysical Research: Atmospheres*, e2022JD037817.

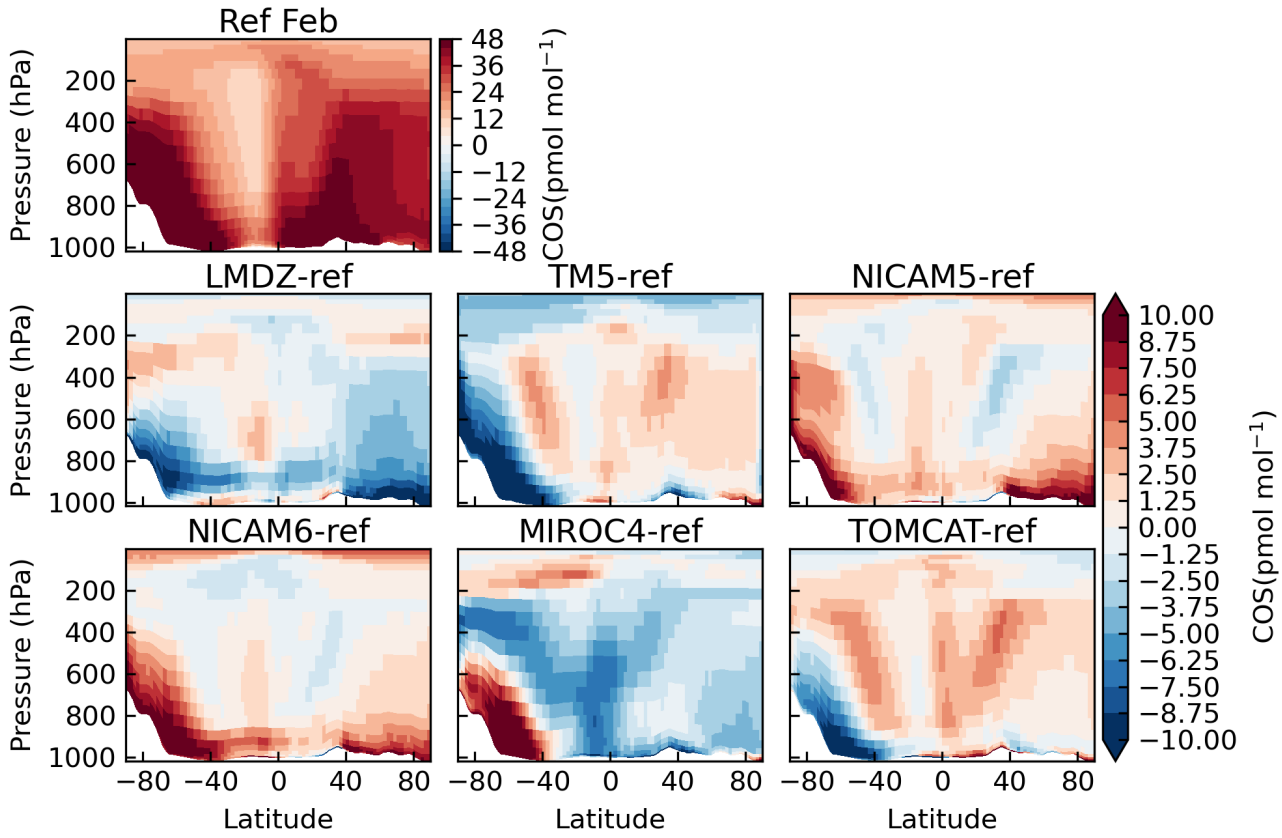

Figure S1. Top row: zonal mean COS mole fraction of the February COS mole fraction averaged over 2010–2018. The reference is the model average, and the model simulations are the difference from the reference. Second and third rows: Zonal mean mole fraction difference between each individual transport model and the reference.

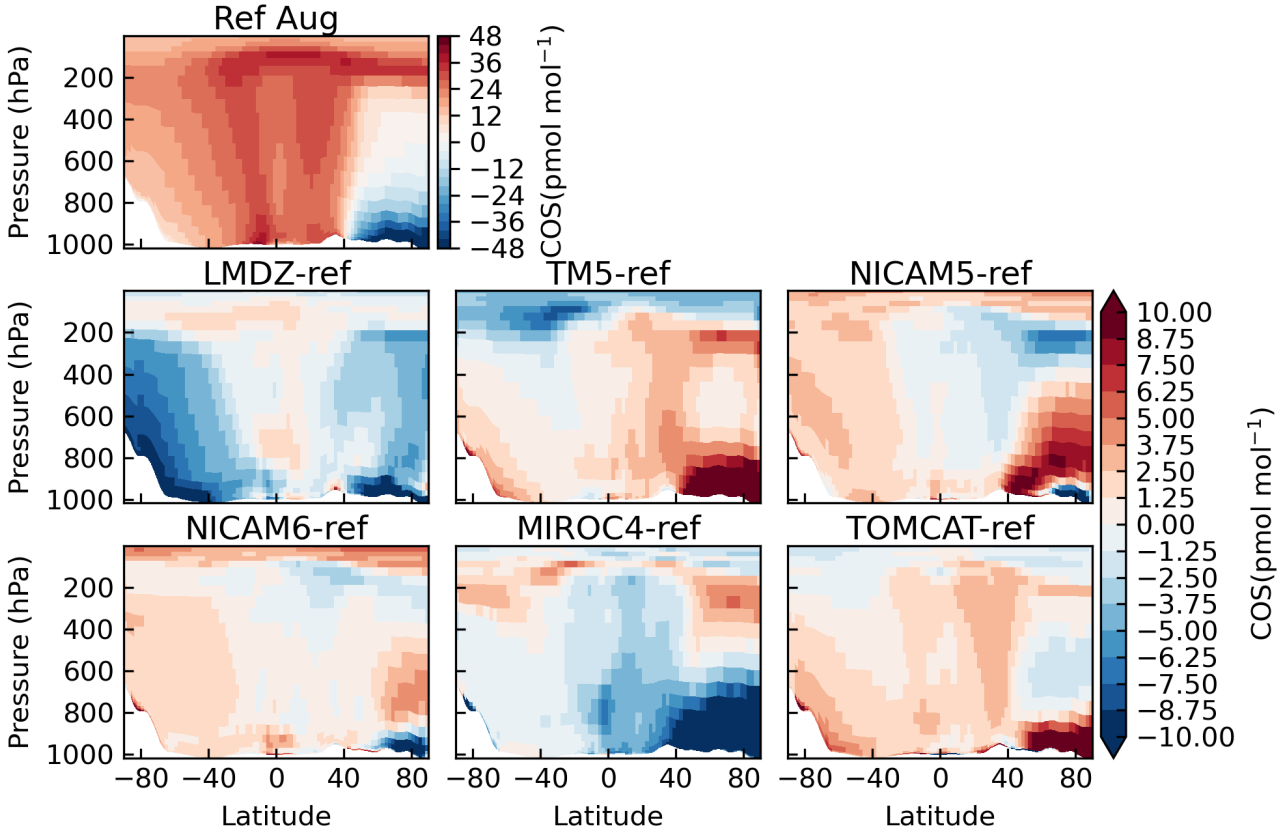

Figure S2. The same as Fig. S1 but for August.

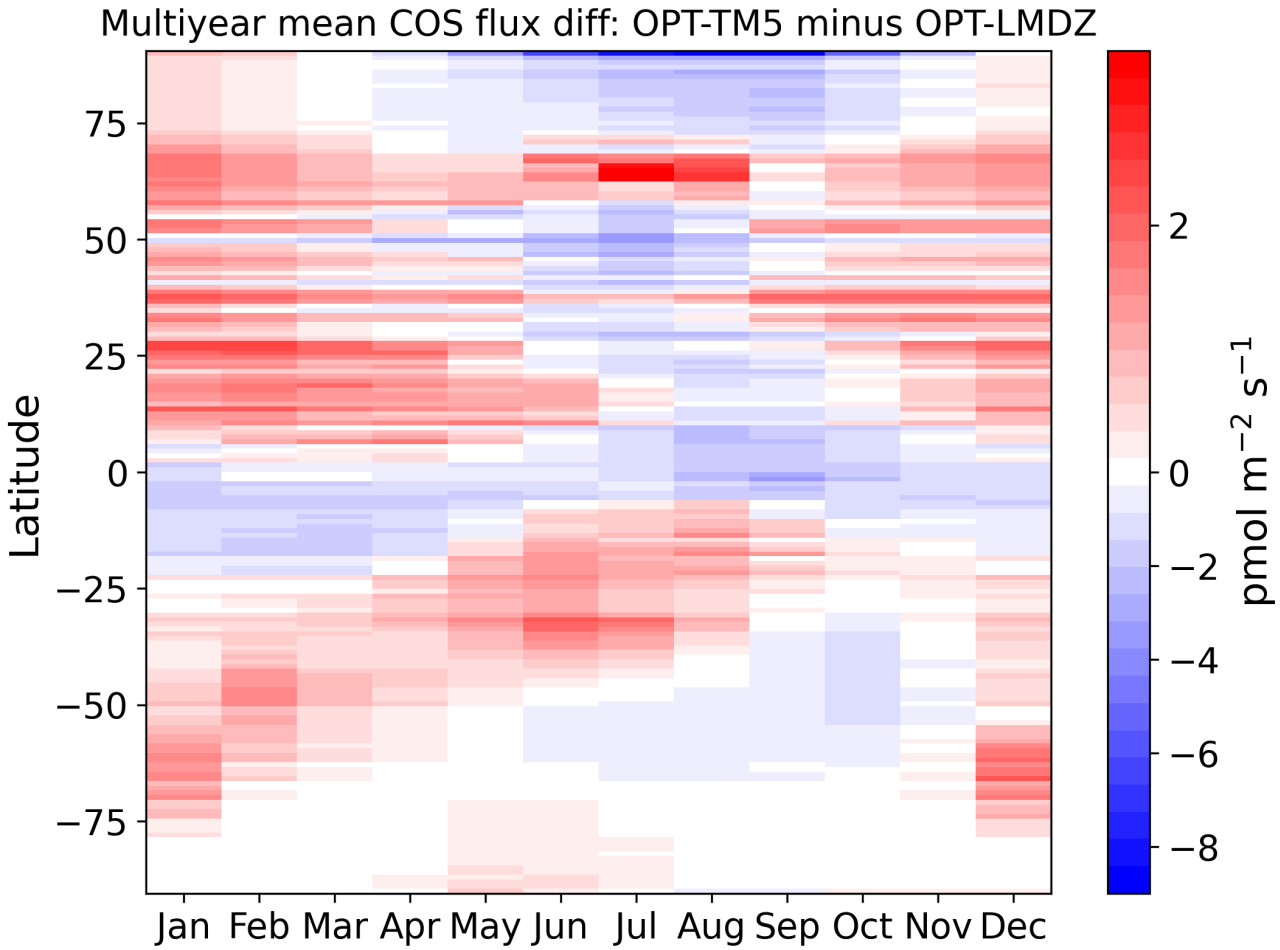

Figure S3. The difference of the temporal-spatial map of the two optimized fluxes defined as TM5 minus LMDz. Note that the positive and negative colorbar scales are not same.

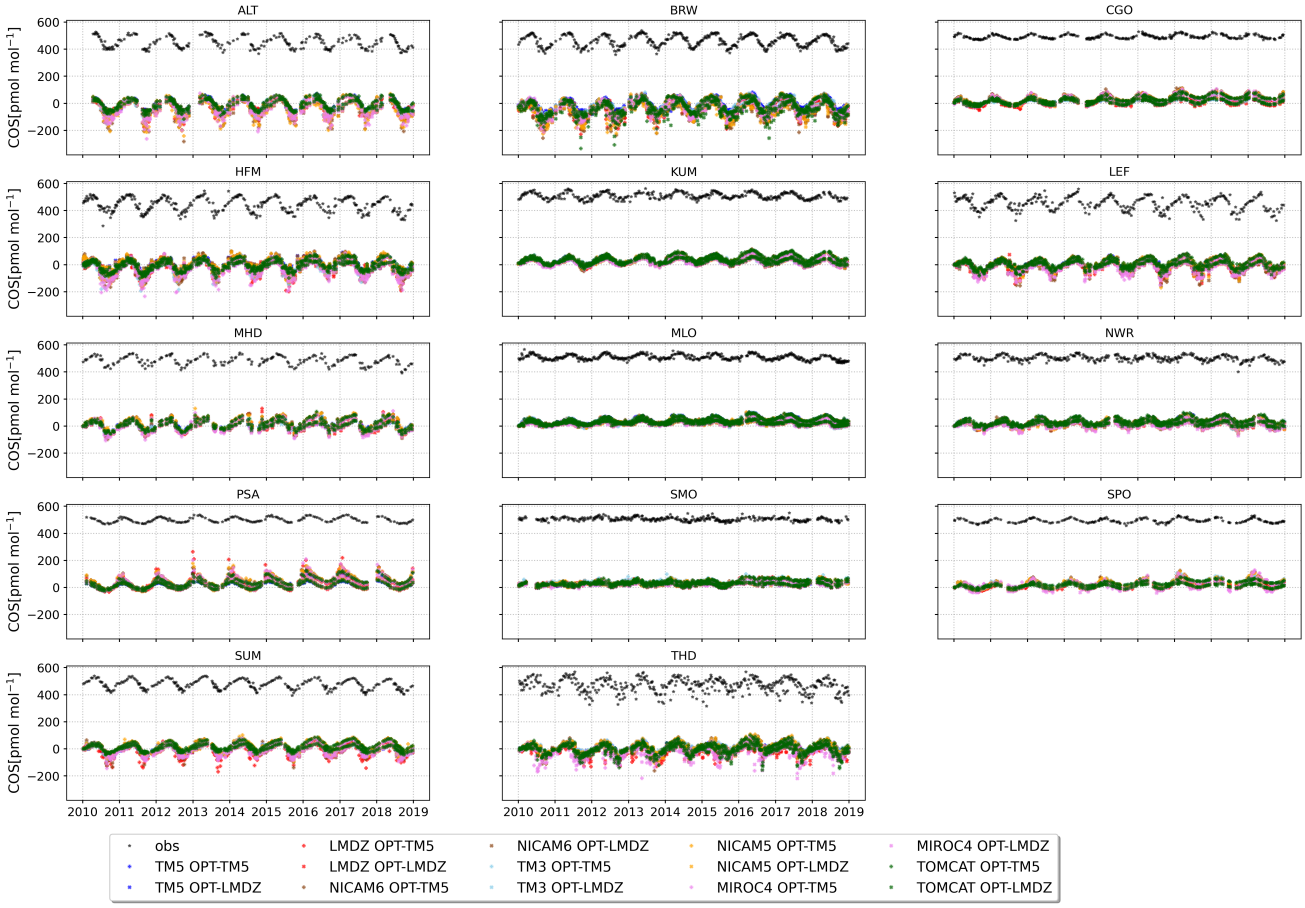

Figure S4. The NOAA surface measurements at 15 stations and the output of the original model simulations.

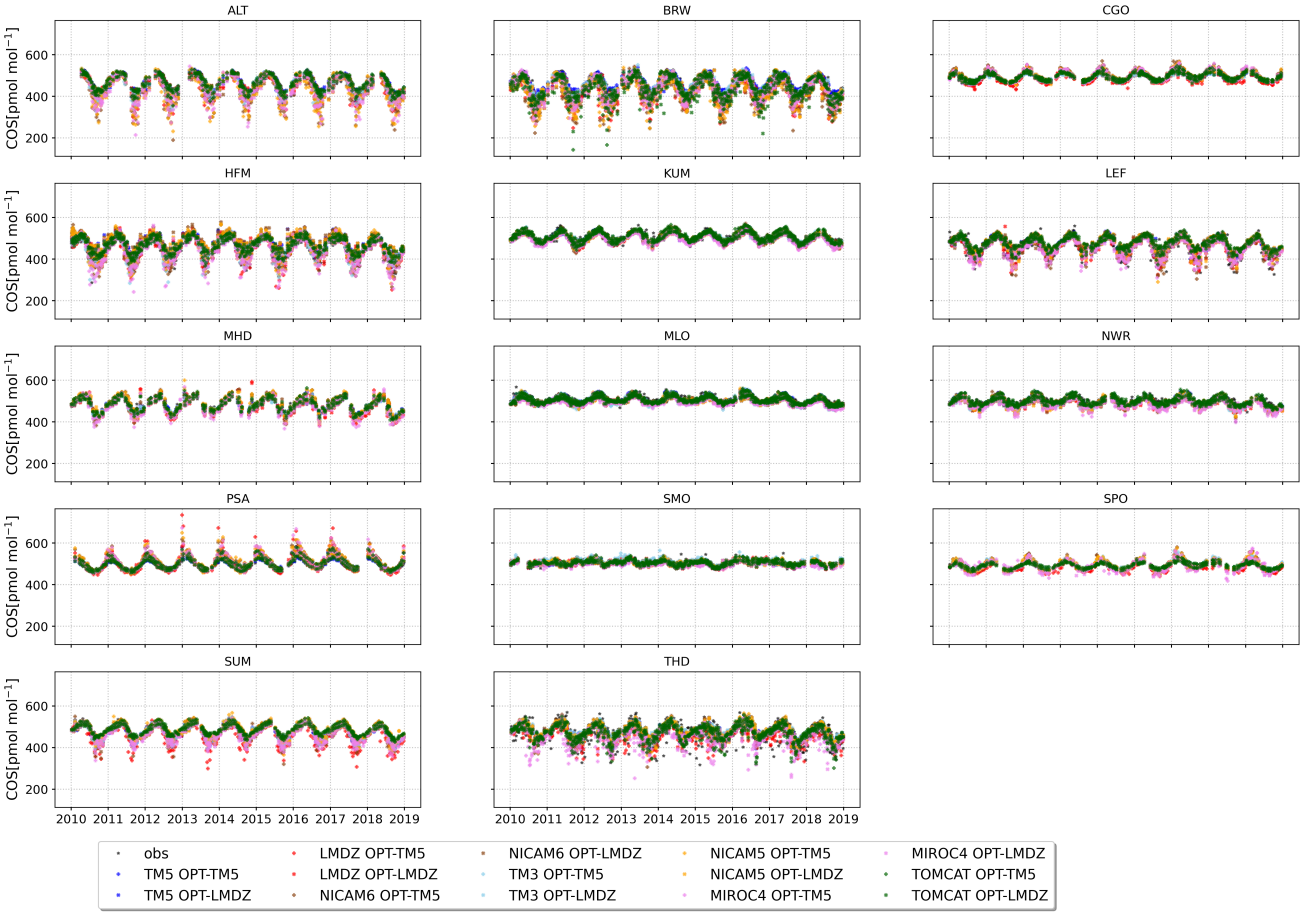

Figure S5. The NOAA surface measurements and the adjusted model outputs. The models are sampled at the times NOAA observations were taken.

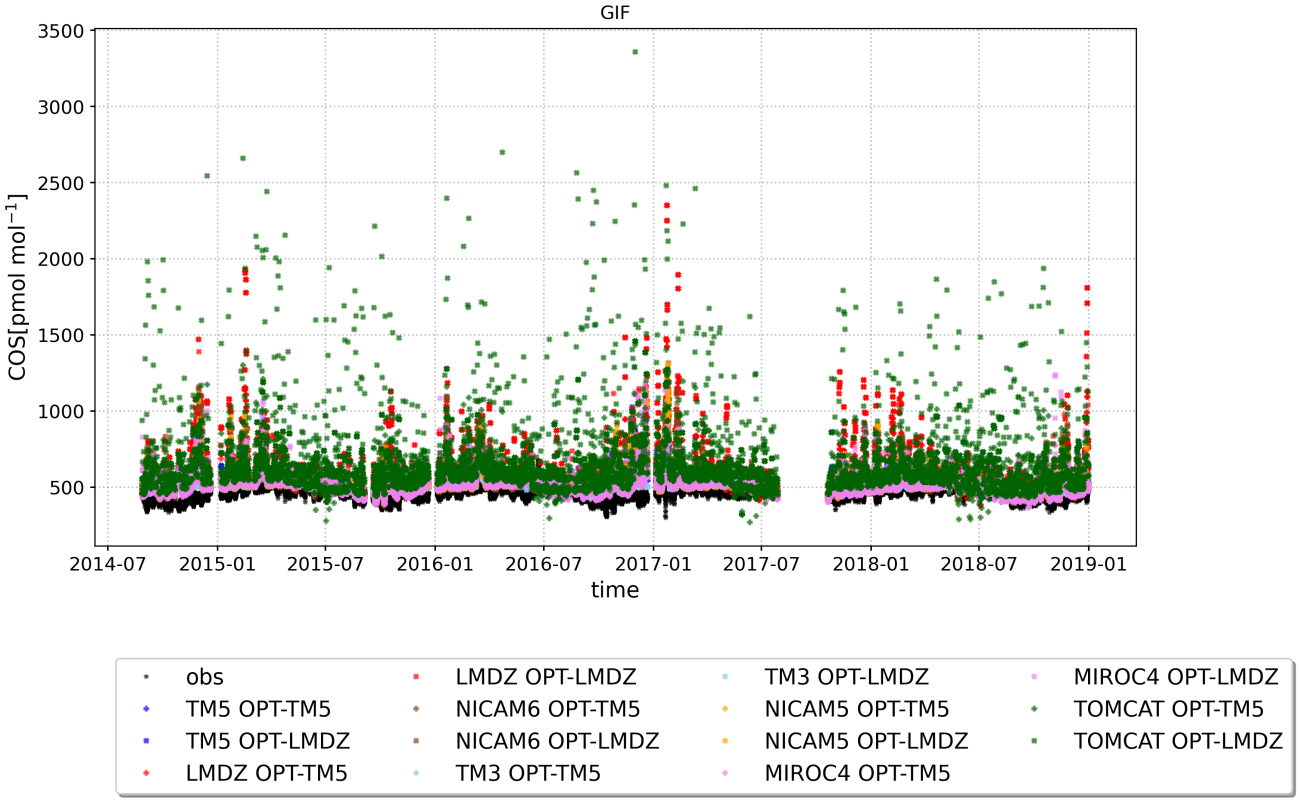

Figure S6. The same as Fig. S5, but for GIF station.

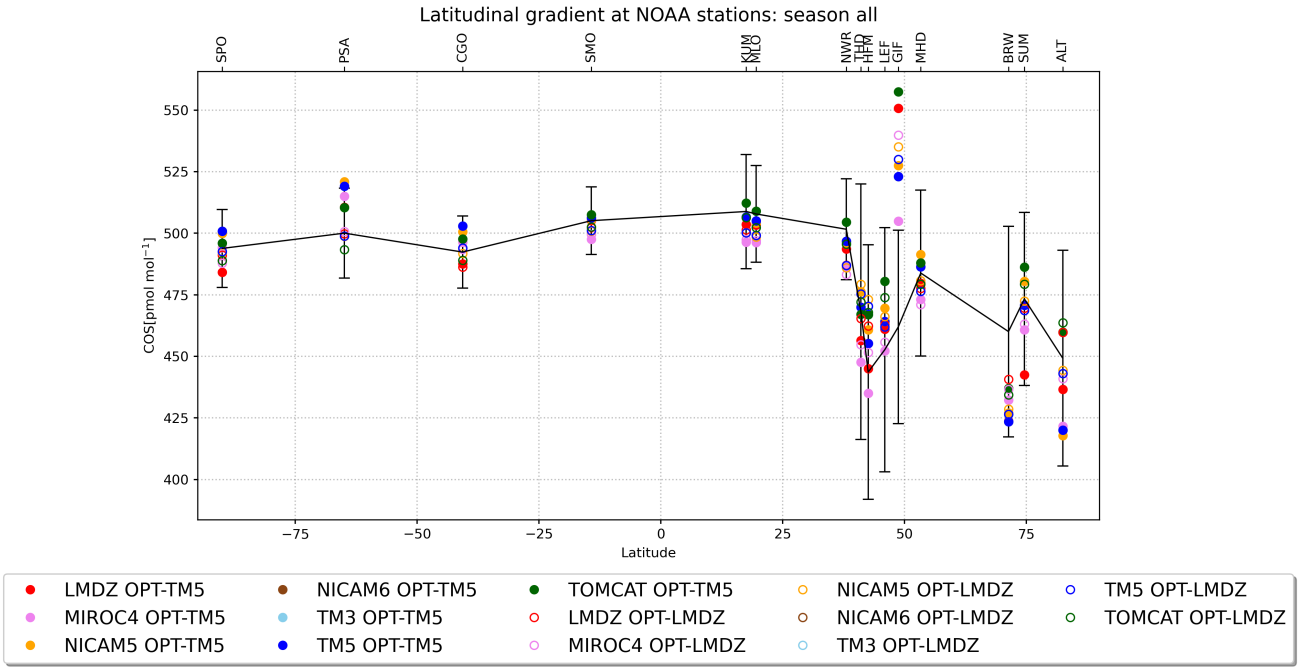

Figure S7. Meridional gradients of single simulations with OPT-TM5 and OPT-LMDz fluxes compared to the NOAA observations. For better visibility, the locations of KUM, NWR, and SUM are shifted -2°N, -2°N, 2°N, respectively. Error bars of the observations correspond to the standard deviation of the measurement time series, and hence include seasonal variability.

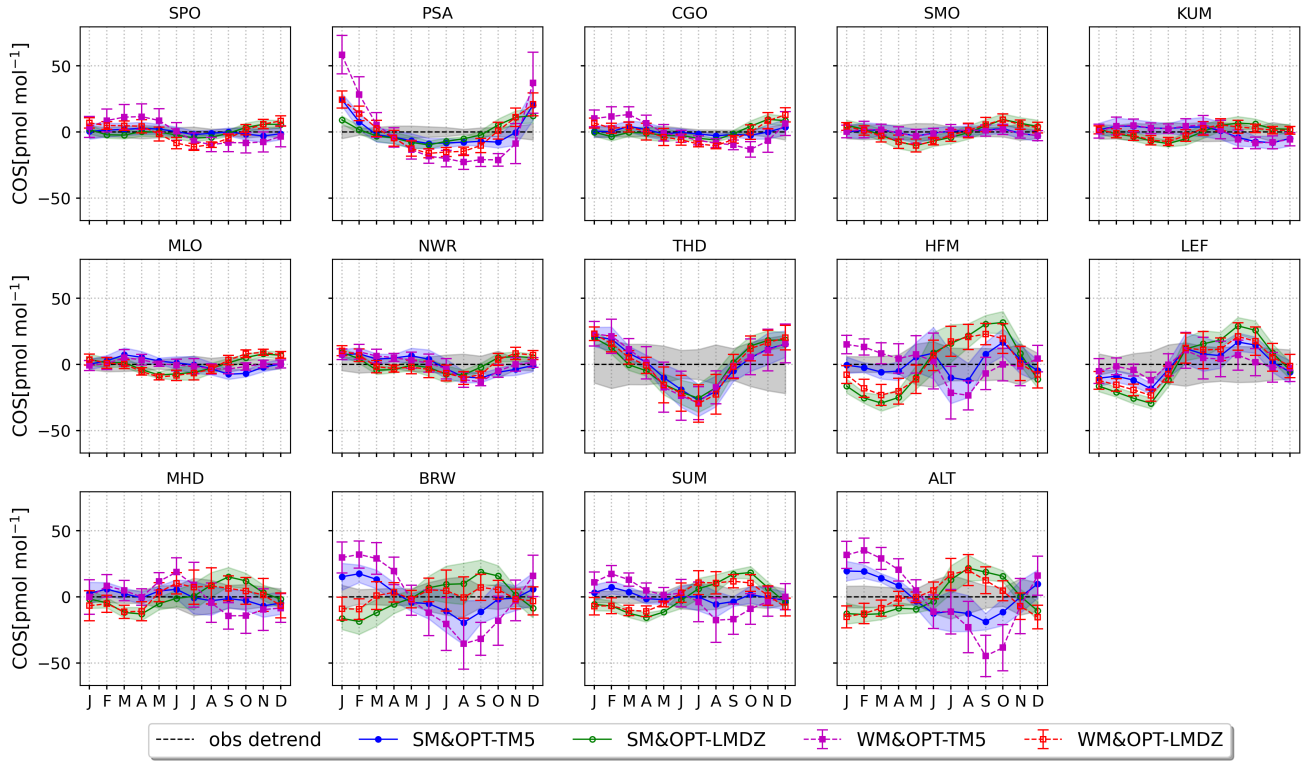

Figure S8. The difference of mean seasonal cycle between the COS abundance simulated by the WM and SM model groups using the optimized fluxes and observed at NOAA surface stations. The COS mole fractions are decomposed with the standard software CCGVU to remove the inter-annual and synoptic variability. The seasonal cycle is averaged over the years 2010–2018. The stations are ordered from SH to NH. The errors of the SM group are shown as shading, and those of the WM group are shown as error-bars. These errors represent the model spread.

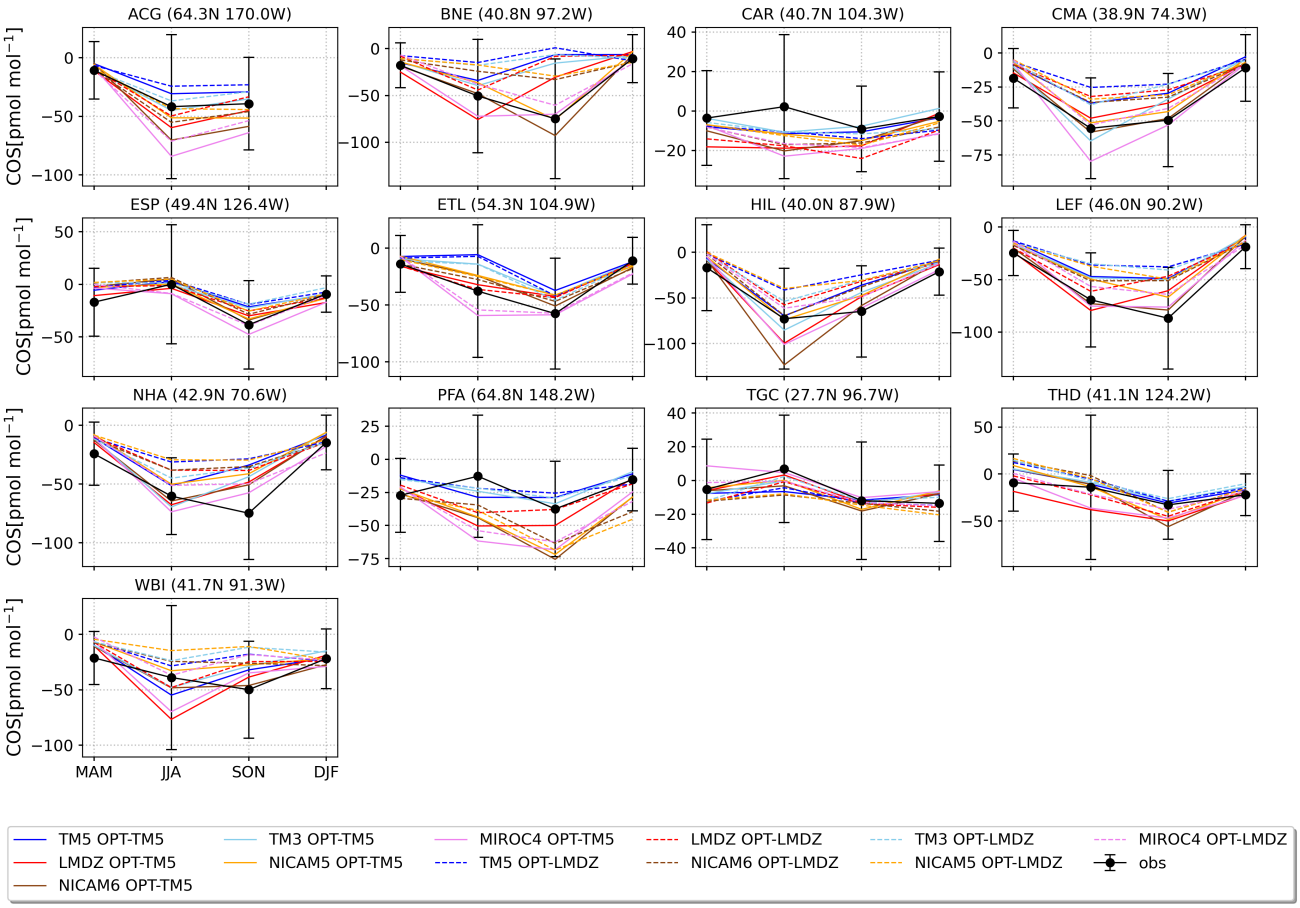

Figure S9. Seasonal mean observed and simulated COS vertical gradient between 1 and 4 km averaged over each NOAA aircraft station in North America. The three-monthly COS gradients are calculated by averaging the differences in COS abundances between 1 and 4 km over all vertical profiles. Error bars represent the standard deviation in the observations. Note that only the LEF and THD surface measurements have been assimilated in the inversions.

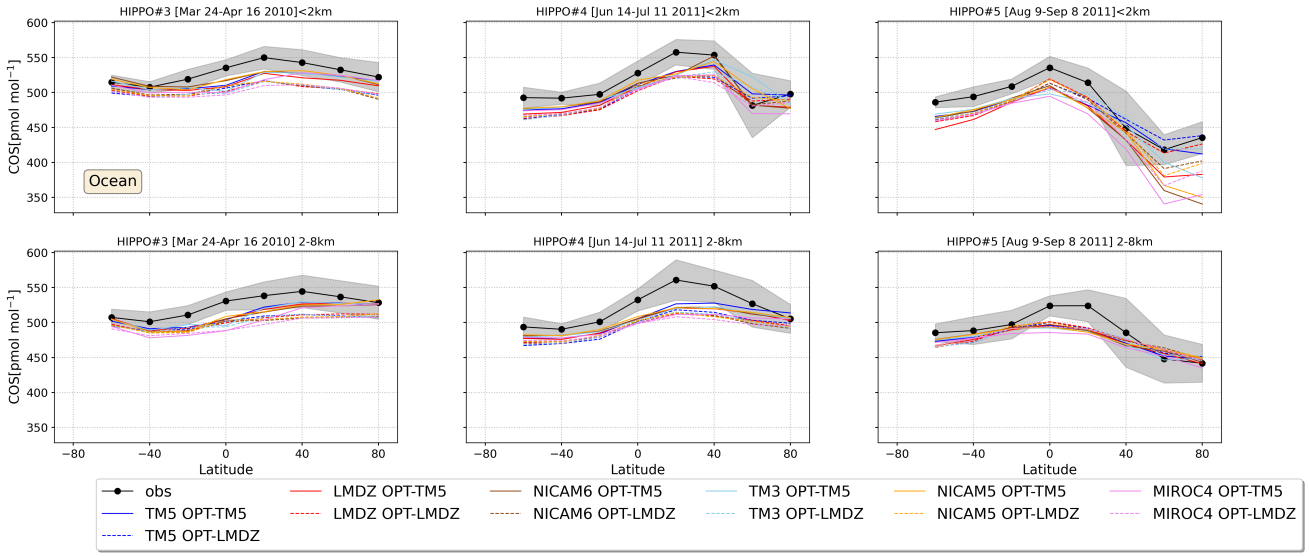

Figure S10. Meridional gradient of HIPPO measurements compared to all individual model simulations over the Pacific Ocean. The data are averaged over the lowest 2 km (upper panels) and between 2 and 8 km (lower panels).

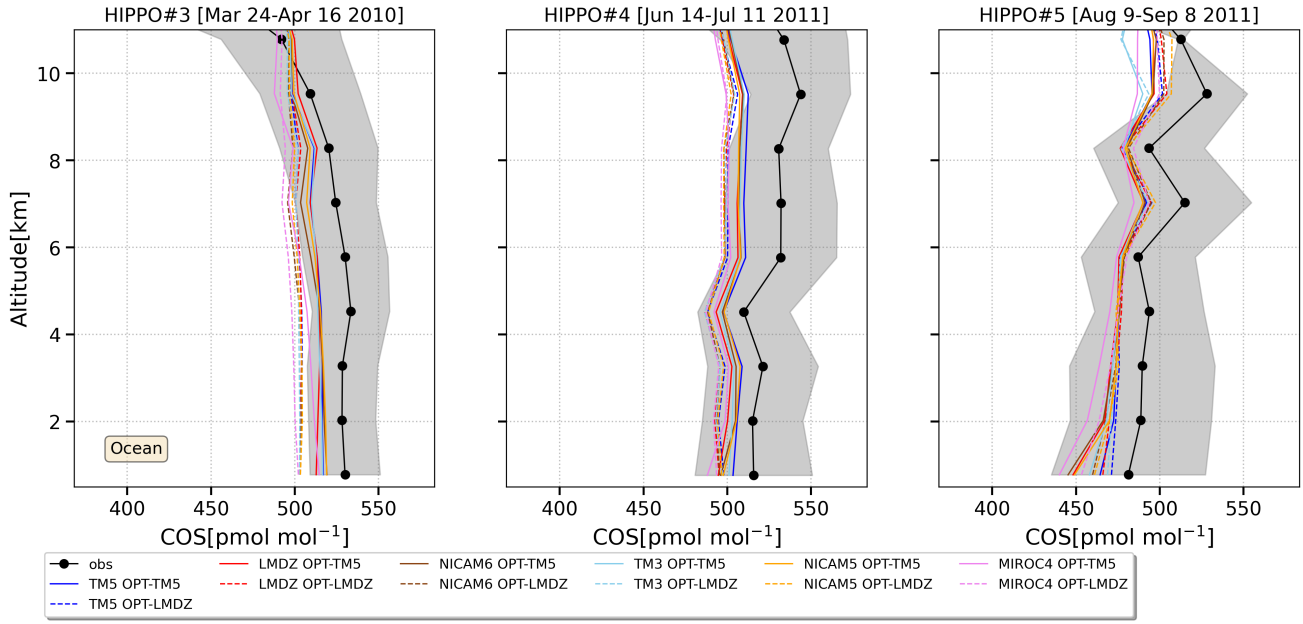

Figure S11. Vertical profiles of HIPPO measurements compared to all individual model simulations over the Pacific Ocean. The vertical data are averaged over 1.25 km bins.

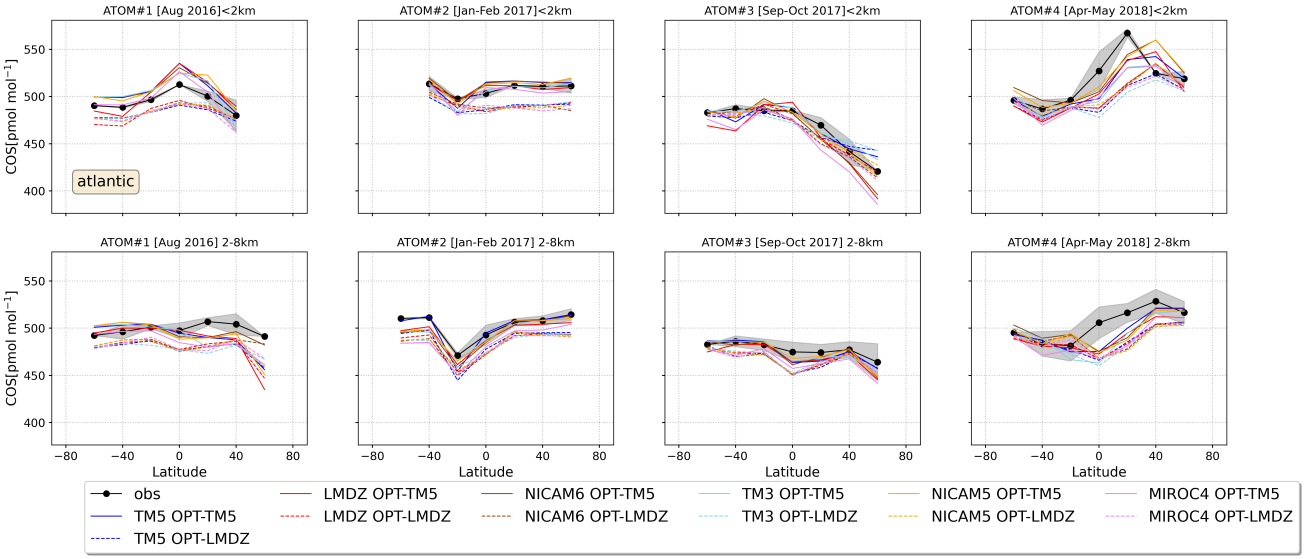

Figure S12. Meridional gradient of ATom measurements compared to all individual model simulations over the Atlantic Ocean. The data are averaged over the lowest 2 km (upper panels) and between 2 and 8 km (lower panels).

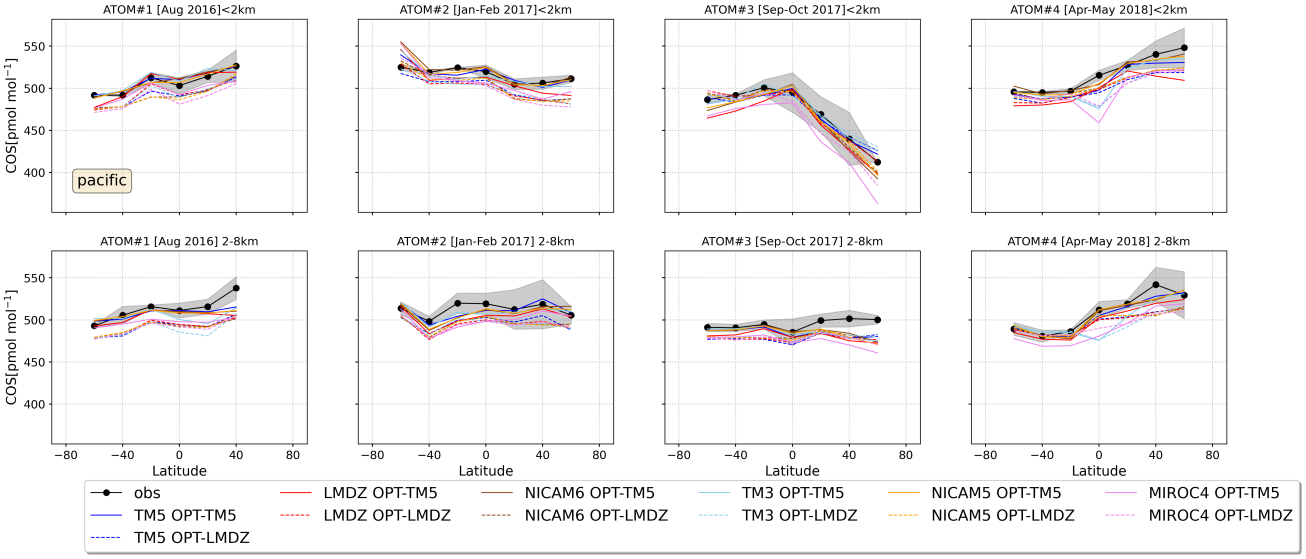

Figure S13. Meridional gradient of ATom measurements compared to all individual model simulations over the Pacific Ocean. The data are averaged over the lowest 2 km (upper panels) and between 2 and 8 km (lower panels).

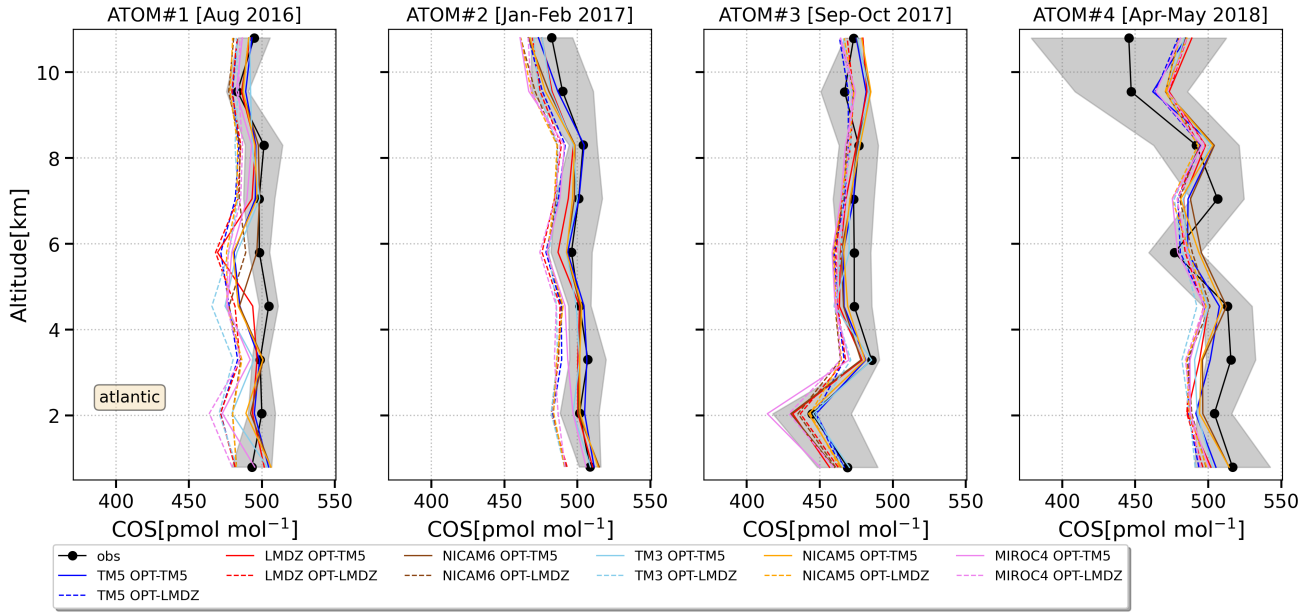

Figure S14. Vertical profiles of ATom measurements compared to all individual model simulations over the Atlantic Ocean. The vertical data are averaged over 1.25 km bins.

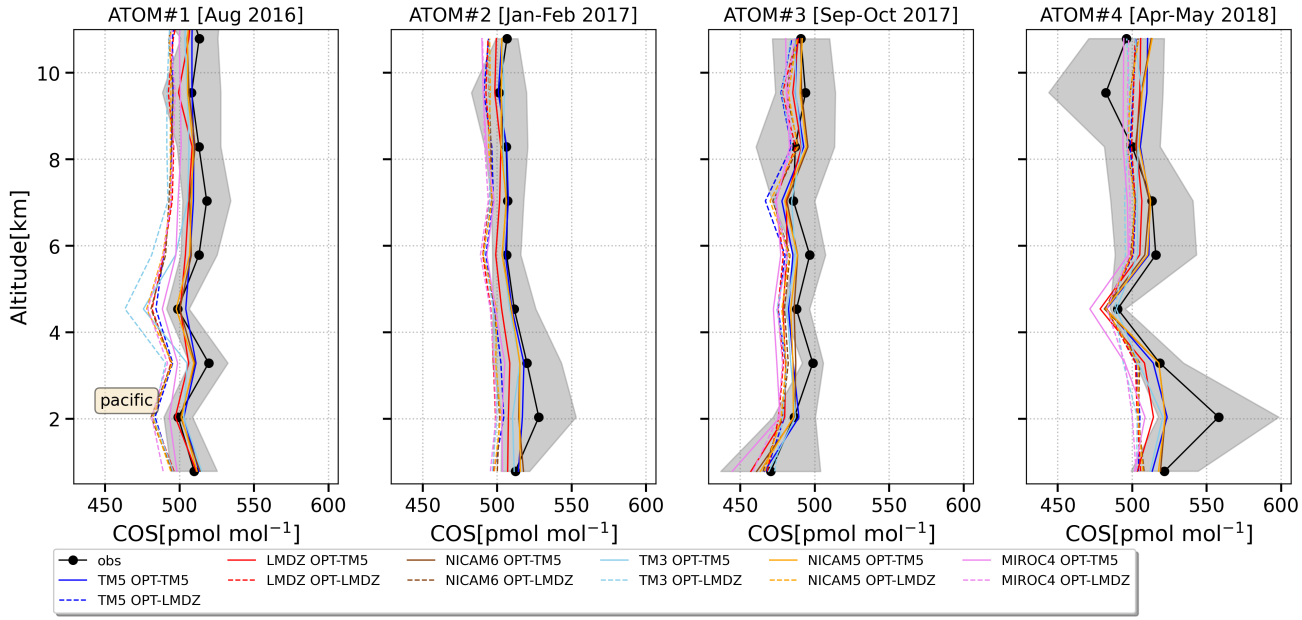

Figure S15. Vertical profiles of ATom measurements compared to all individual model simulations over the Pacific Ocean. The vertical data are averaged over 1.25 km bins.

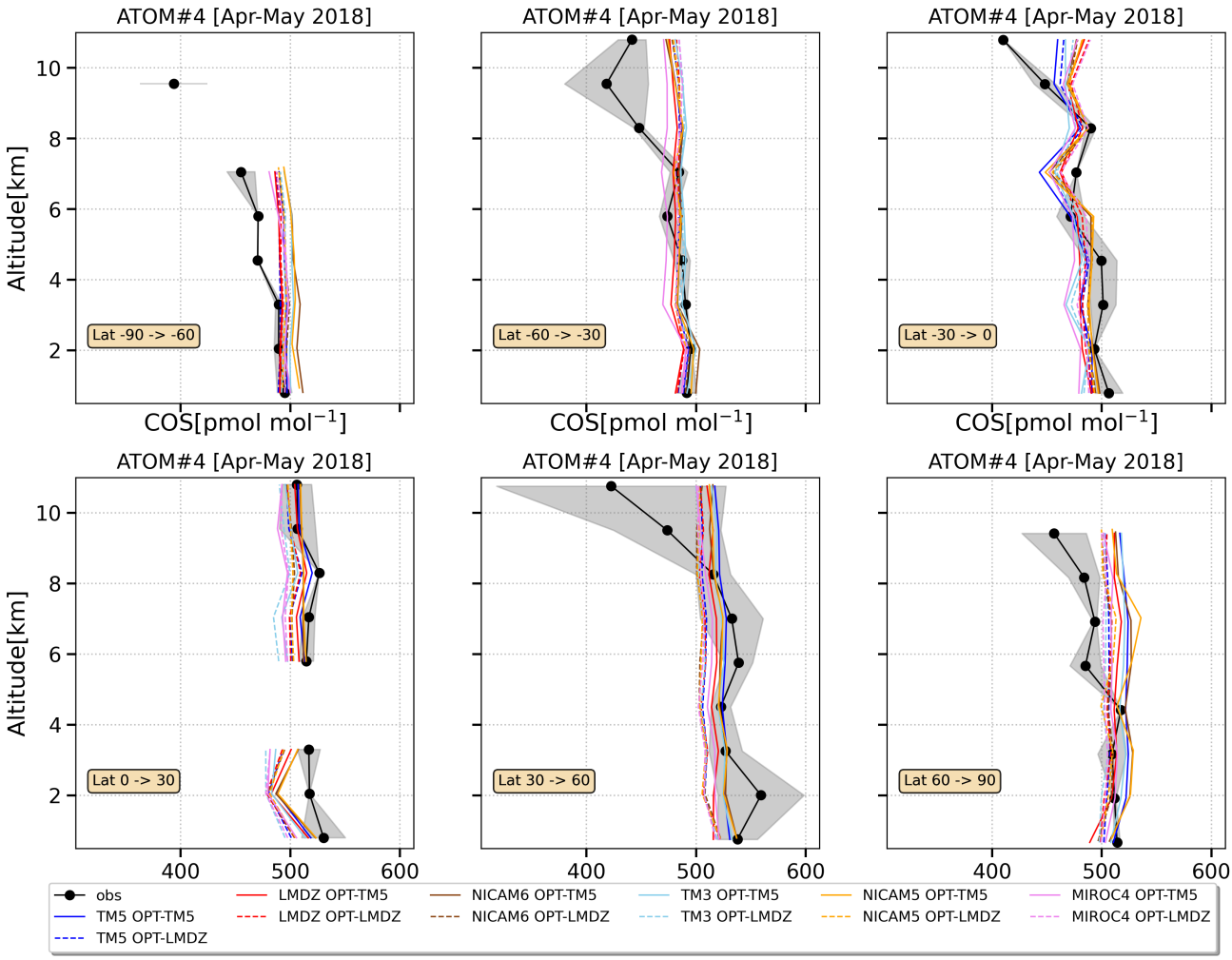

Figure S16. Vertical profiles of the ATom4 measurements compared to all individual model simulations. The vertical data are averaged over 1.25 km bins. The data are further stratified according to latitude ranges.

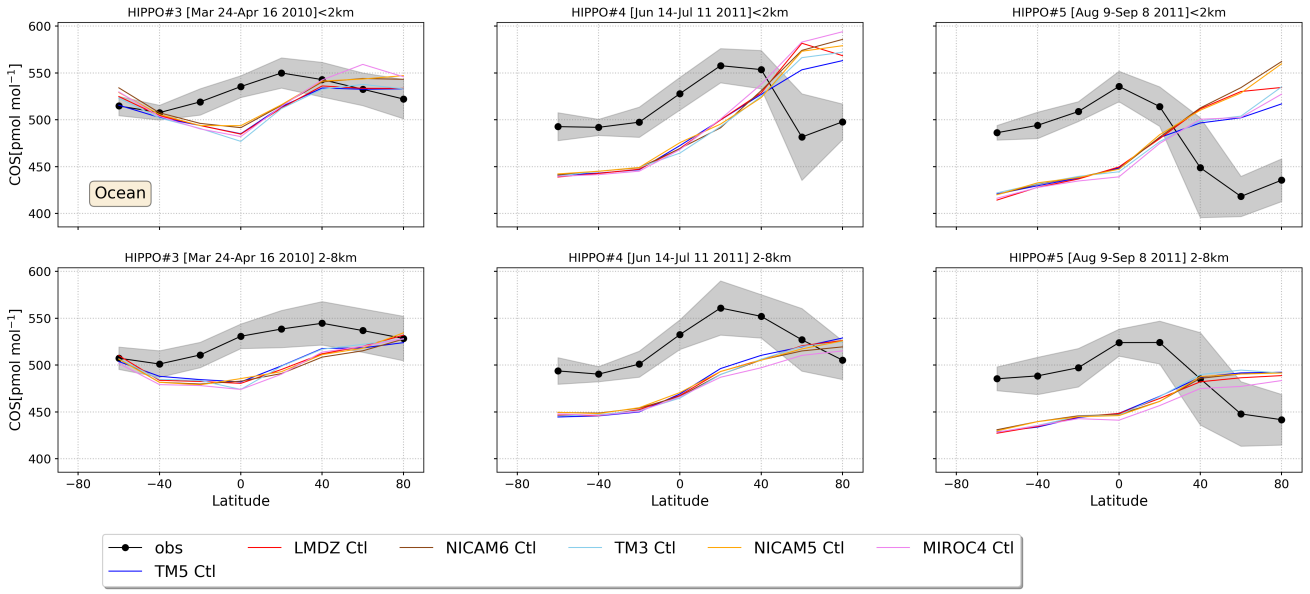

Figure S17. Meridional gradients of HIPPO and all individual simulations using the control flux scenario over the Ocean (Pacific).

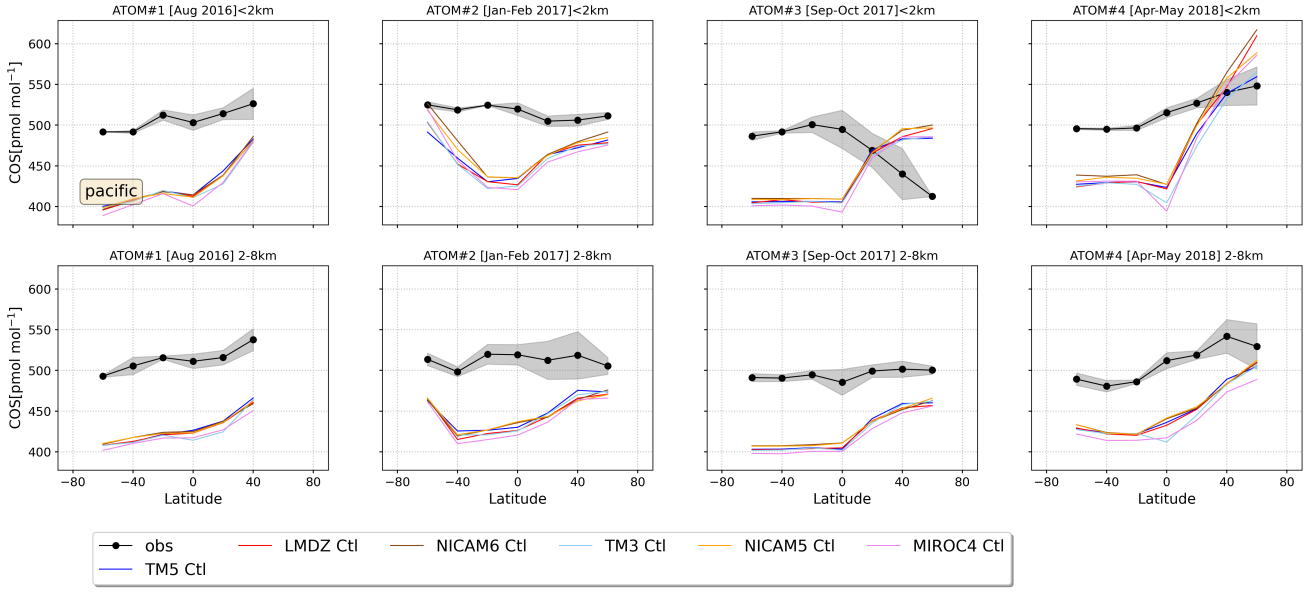

Figure S18. Meridional gradients of ATom and all individual simulations using the control flux scenario over the Pacific.

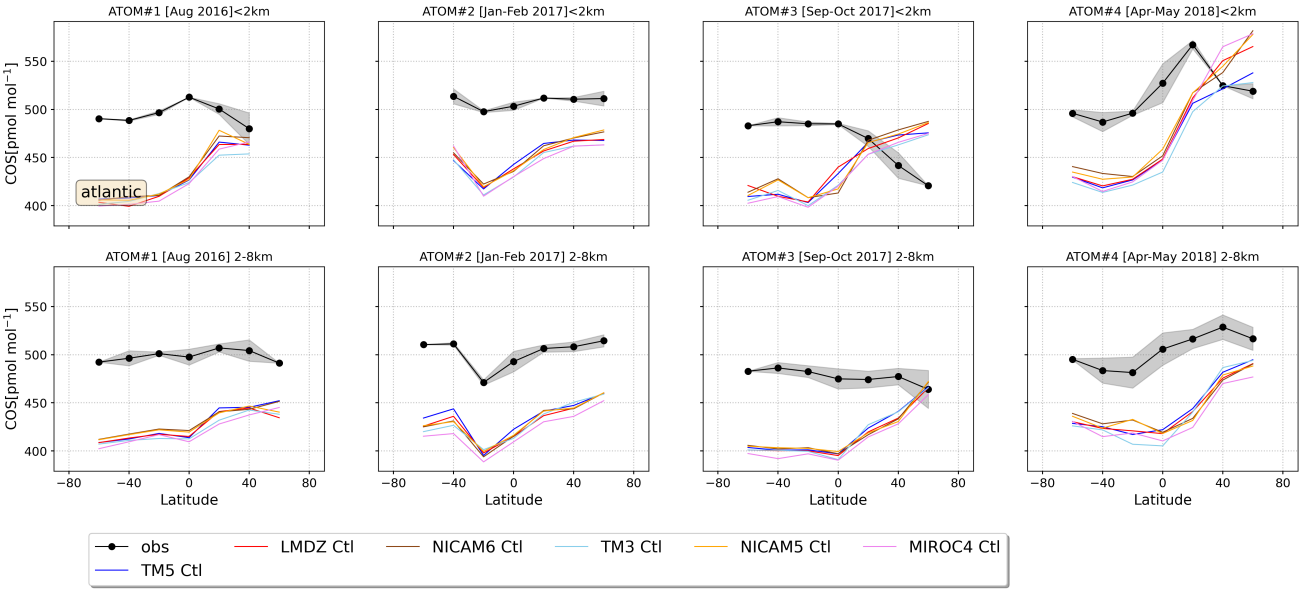

Figure S19. The same as Fig. S18, but over the Atlantic.